Laser-induced breakdown and damage in bulk transparent materials induced by tightly focused femtosecond laser pulses

2001 Meas. Sci. Technol. 12 1784

(http://iopscience.iop.org/0957-0233/12/11/305)

INSTITUTE OF PHYSICS PUBLISHING MEASUREMENT SCIENCE AND TECHNOLOGY
Meas. Sci. Technol. **12** (2001) 1784–1794 PII: S0957-0233(01)26160-8

Laser-induced breakdown and damage in bulk transparent materials induced by tightly focused femtosecond laser pulses

Chris B Schaffer, André Brodeur and Eric Mazur

Harvard University, Department of Physics and Division of Engineering and Applied Sciences, Cambridge, MA 02138, USA

E-mail: chris_schaffer@post.harvard.edu and mazur@physics.harvard.edu

Received 25 June 2001, accepted for publication 21 August 2001
Published 9 October 2001
Online at stacks.iop.org/MST/12/1784

Abstract
Laser-induced breakdown and damage to transparent materials has remained an active area of research for four decades. In this paper we review the basic mechanisms that lead to laser-induced breakdown and damage and present a summary of some open questions in the field. We present a method for measuring the threshold intensity required to produce breakdown and damage in the bulk, as opposed to on the surface, of the material. Using this technique, we measure the material band-gap and laser-wavelength dependence of the threshold intensity for bulk damage using femtosecond laser pulses. Based on these thresholds, we determine the relative role of different nonlinear ionization mechanisms for different laser and material parameters.

Keywords: laser-induced breakdown, damage threshold, femtosecond laser, laser micromachining, optical damage

1. Introduction

Laser-induced breakdown and damage in transparent materials have been studied since the advent of high-power pulsed lasers [1]. Despite this long history, much still remains to be learned about the interaction of high-intensity laser pulses with transparent materials. The availability of laser pulses with femtosecond duration allows materials to be subjected to a higher laser intensity than ever before, opening the door to the study of laser/material interactions in a new regime. From a practical point of view, this high laser intensity offers new challenges and provides new opportunities. The peak power in large femtosecond laser systems is currently limited by the damage threshold of the optics in the laser chain [2]. Understanding the mechanisms responsible for optical damage may allow higher-damage-threshold optics to be constructed for these laser systems. Additionally, in recent years, the structural alterations produced in transparent materials by ultrashort laser pulses have been used for micromachining [3–7]. A better grasp of the nonlinear ionization mechanisms at play may allow for higher-precision micromachining and more control over the changes induced in the material.

In a transparent material, there is no linear absorption of the incident laser light. For optical breakdown and material damage to occur, a nonlinear absorption mechanism must deposit laser energy into the material by promoting electrons from the valence band to the conduction band. There are two classes of nonlinear excitation mechanisms that play a role in this absorption, photoionization and avalanche ionization. If enough laser energy is deposited into the material by these nonlinear absorption mechanisms, permanent damage is produced.

1.1. Nonlinear photoionization

Photoionization refers to direct excitation of the electron by the laser field. Because a single photon of visible light does not have enough energy to excite an electron in a transparent material from the valence to the conduction band, multiple photons are required to excite the electron. Depending on the laser frequency and intensity, there are two different regimes

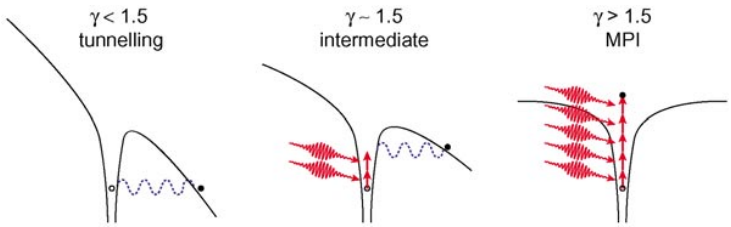

Figure 1. Schematic diagram of the photoionization of an electron in an atomic potential for different values of the Keldysh parameter. In a solid, the electron is promoted from the valence to the conduction band, rather than ionized.

of photoionization, the multiphoton ionization regime and the tunnelling ionization regime. Keldysh showed that both multiphoton and tunnelling regimes could be described within the same framework [8]. The conceptual picture and the approximations used in calculations for these two mechanisms are very different, however.

In tunnelling ionization, the electric field of the laser suppresses the Coulomb well that binds a valence electron to its parent atom. If the electric field is very strong, the Coulomb well can be suppressed enough that the bound electron tunnels through the short barrier and becomes free, as shown schematically in the left-hand panel of figure 1. This type of nonlinear ionization dominates for strong laser fields and low laser frequency.

At high laser frequencies (but still below that required for single photon absorption) nonlinear ionization occurs due to the simultaneous absorption of several photons by an electron, as shown in the right-hand panel of figure 1. To be promoted from the valence to the conduction band by this multiphoton absorption, the electron must absorb enough photons so that the number of photons absorbed times the photon energy is equal to or greater than the band-gap of the material.

The transition between multiphoton ionization and tunnelling ionization was expressed by Keldysh in terms of the adiabatic parameter, also known as the Keldysh parameter [8],

$$\gamma = \frac{\omega}{e}\left[\frac{mcn\varepsilon_0 E_g}{I}\right]^{1/2} \tag{1}$$

where ω is the laser frequency, I is the laser intensity at the focus, m and e are the reduced mass and charge of the electron, c is the velocity of light, n is the refractive index of the material, E_g is the band-gap of the material and ε_0 is the permitivity of free space. When the Keldysh parameter is larger (smaller) than about 1.5, photoionization is a multiphoton (tunnelling) process. In the intermediate regime, the photoionization is a mix between tunnelling and multiphoton ionization as depicted in the middle panel of figure 1.

The photoionization rate depends strongly on laser intensity. In the multiphoton ionization regime, the rate is $P(I)_{MPI} = \sigma_k I^k$ where σ_k is the multiphoton absorption coefficient for absorption of k photons [9]. The number of photons required is determined by the smallest k which satisfies the relation $k\hbar\omega \geqslant E_g$. The tunnelling rate, on the other hand, scales more weakly with the laser intensity than the multiphoton rate.

Figure 2 shows the photoionization rate and Keldysh parameter as a function of laser intensity for 800 nm light in fused silica (7.5 eV band-gap). The dashed, dotted and solid lines represent the photoionization rate for mulitphoton ionization only (equation (40) in [8]), tunnelling ionization only (equation (41) in [8]) and the full Keldysh expression (equation (37) in [8]), respectively. The multiphoton only rate and the tunnelling only rate agree with each other and with the complete rate for a Keldysh parameter of about 1.5. The rate based on tunnelling only agrees with the complete formula up to a Keldysh parameter of just over 1.5, then overestimates the rate. Similarly, the rate based on multiphoton ionization only agrees with the full formula for Keldysh parameters down to just below 1.5, then underestimates the rate. Simulations for other laser wavelength and material band-gap consistently show this very abrupt transition from a multiphoton to tunnelling regime at a Keldysh parameter of about 1.5.

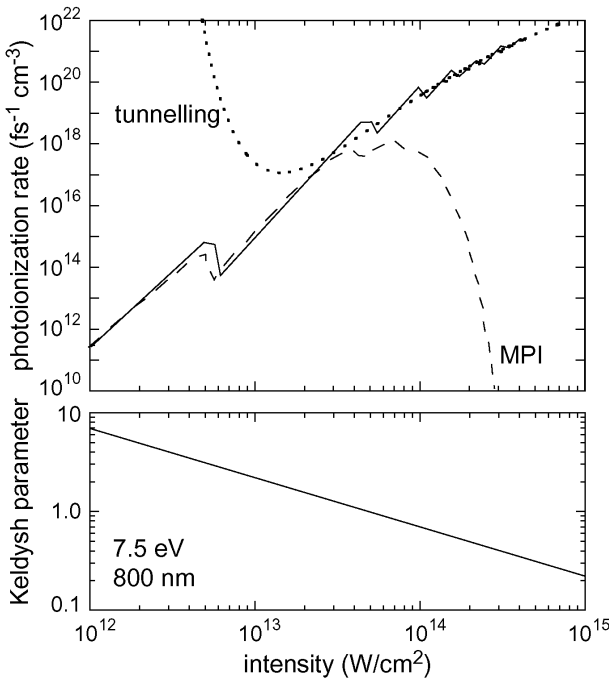

Figure 2. Photoionization rate and Keldysh parameter as a function of laser intensity for 800 nm light in fused silica (7.5 eV band-gap). The solid line represents the photoionization rate based on the full expression from Keldysh (equation (37) in [8]), the dashed line represents the multiphoton ionization rate, and the dotted line represents the tunnelling ionization rate. Note that the multiphoton and tunnelling rates overlap around a Keldysh parameter of 1.5.

Some recent experiments have called Keldysh's theory into question. Lenzner *et al* found that they cannot account for the pulse duration dependence of the surface damage threshold of fused silica with the ionization rates predicted by Keldysh, and that the multiphoton ionization coefficients that

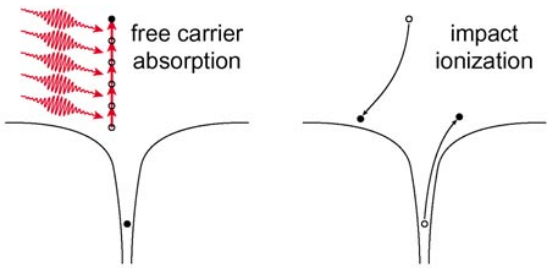

Figure 3. Schematic diagram of avalanche ionization. An initially free electron linearly absorbs several laser photons through free-carrier absorption, then impact ionizes another electron. As in figure 1, the electrons are promoted from the valence to the conduction band rather than ionized in a solid.

best fit their data are several orders of magnitude smaller than those predicted by Keldysh's theory [10]. This discrepancy could result from electron dephasing due to frequent phonon scattering [11]. Other researchers, however, have successfully fitted their data using rates from Keldysh's theory [12, 13].

1.2. Avalanche ionization

Avalanche ionization involves free-carrier absorption followed by impact ionization. An electron already in the conduction band of the material linearly absorbs several laser photons sequentially, moving to higher energy states in the conduction band, illustrated in the left-hand panel of figure 3. In order to conserve both energy and momentum, the electron must transfer momentum by absorbing or emitting a phonon or scattering off an impurity when it absorbs a laser photon [14]. For electrons high in the conduction band, the deformation potential scattering time is approximately 1 fs, so frequent collisions make free carrier absorption efficient [15]. After the sequential absorption of n photons, where n is the smallest number which satisfies the relation $n\hbar\omega \geqslant E_g$, the electron's energy excedes the conduction band minimum by more than the band-gap energy. The electron can then collisionally ionize another electron from the valence band, as illustrated in the right-hand panel of figure 3. The result of the collisional ionization is two electrons near the conduction band minimum, each of which can absorb energy through free-carrier absorption and subsequently impact ionize additional valence band electrons. As long as the laser field is present, the electron density, N, in the conduction band grows according to

$$\frac{\mathrm{d}N}{\mathrm{d}t} = \eta N \tag{2}$$

where η is the avalanche ionization rate.

Avalanche ionization requires some 'seed' electrons in the conduction band of the material. These initial electrons are provided either by thermally excited carriers, by easily ionized impurity or defect states, or by carriers that are directly photoexcited by multiphoton or tunnelling ionization.

Stuart *et al* developed a model of avalanche ionization in which the avalanche rate depends linearly on the laser intensity (i.e. $\eta = \alpha I$, where α is the avalanche ionization coefficient) [12]. Heating of the electrons in the conduction band is taken into account using what is basically a Drude model but with the electron energy dependence of the conductivity included. The model then makes the flux doubling approximation, which states that an electron in the conduction impact ionizes an electron from the valence band as soon as it has enough energy to do so. In other words, the model assumes there are no electrons in the conduction band with energy higher than the conduction band minimum plus the band-gap energy (at least until the material is fully ionized, after which further electron heating can occur). Stuart's model also assumes that the energy distribution of electrons in the conduction band does not change shape as the electron density grows. Some researchers have called this model into question [11, 16]. Thornber, for example, predicts an avalanche rate that depends on the square root of the laser intensity [17].

1.3. Damage mechanisms—picosecond to nanosecond pulses

When the absorption mechanisms described above deposit sufficient energy into the material, permanent damage is produced. For pulse durations longer than a few tens of picoseconds, energy is transfered from the laser-excited electrons to the lattice on the time scale of the pulse duration. This energy is then carried out of the focal volume by thermal diffusion. Damage occurs when the temperature of the material in the irradiated region becomes high enough for the material to melt or fracture [13]. Energy is deposited into the material by the laser pulse and is transported out of the irradiated region by thermal diffusion, thus it is the relative rate of energy deposition and thermal diffusion that determines the damage threshold. Simple calculations show that, in this case, the threshold fluence for optical damage scales as the square root of the pulse duration [18]. Soileau *et al* were the first to observe a departure from this dependence for pulses shorter than 10 ps [19].

For damage caused by pulses longer than a few tens of picoseconds, the source of the initial conduction-band electrons that seed the avalanche ionization is very important. Avalanche ionization is very efficient for such pulses because the long pulse duration allows more time for exponential growth of the electron density. Because avalanche ionization is so efficient, the laser intensity required to produce damage is not high enough to directly photoionizing electrons, so either thermally excited electrons or impurity and defect states provide the initial seed electrons for the avalanche. A high concentration of easily ionized impurity electrons lowers the threshold for optical damage compared to that of the pure material, making determination of the intrinsic breakdown threshold difficult [20].

The dependence of the breakdown threshold on the presence of impurity electrons in the conduction band also makes the threshold for optical breakdown and damage non-deterministic. Typical impurity concentrations of electrons in the conduction band of a transparent solid are about 10^8 cm^{-3} [15]. A laser beam focused to a 10 μm diameter spot inside the material has a Raleigh range of about 75 μm, and therefore a focal volume of about 10^{-8} cm^3. On average there is therefore about one impurity electron in the conduction band in the focal volume. Because the seed electrons are so critical for the breakdown process with long pulses, small fluctuations in the number of seed electrons in the focal volume strongly affect the breakdown process. For a constant laser energy that is near

the threshold, some laser shots produce damage while others do not, depending on how many seed electrons are in the focal volume of each laser shot.

1.4. Damage mechanisms—sub-picosecond pulses

For pulses shorter than a few picoseconds, the mechanism for optical damage is simpler than for longer laser pulses. Absorption occurs on a time scale that is short compared to the time scale for energy transfer to the lattice, decoupling the absorption and lattice heating processes [12]. Electrons in the conduction band are heated by the laser pulse much faster than they can cool by phonon emission. The electron density grows through avalanche ionization until the plasma frequency approaches the frequency of the incident laser radiation (the 'critical' plasma density) [12]. This high density plasma strongly absorbs laser energy by free-carrier absorption. The reflectivity of the plasma at the critical density is only a few per cent, so most of the laser energy is transmitted into the plasma where it can be absorbed. At higher plasma densities, however, a significant fraction of the laser pulse energy can be reflected. Only after the laser pulse is gone is energy transferred from the electrons to the lattice. This shocklike deposition of energy, on a time scale much shorter than the thermal diffusion time, leads to ablation of material on the surface or permanent structural change in the bulk.

For sub-picosecond laser pulses, photoionization plays an important role in the generation of conduction band electrons. Photoionization by the leading edge of the laser pulse provides the seed electrons for avalanche ionization during the rest of the pulse [12]. This self-seeded avalanche makes short-pulse breakdown less dependent on defects in the material than long-pulse breakdown and therefore the threshold for short-pulse damage is deterministic [20]. For very short laser pulses, photoionization can dominate avalanche ionization and produce a sufficient plasma density to cause damage by itself [10, 12].

Damage produced by pulses in the femtosecond range is far more regular from shot to shot and more confined than with longer pulses [4]. Because short pulses require less energy than longer pulses to reach the intensity necessary to produce optical breakdown, they deposit less energy in the material. Less energy deposition leads to more precise ablation or bulk material modification. This deterministic breakdown and damage near threshold and controllable material alteration make femtosecond lasers an ideal tool for micromachining [3].

1.5. Open questions about laser-induced breakdown

The review presented above highlights several open questions that need to be addressed. The validity of Keldysh's theory for photoionization needs to be determined, and the scaling of the avalanche ionization rate with laser intensity needs to be established. From an experimental point of view, these issues can be addressed by measuring the breakdown threshold as a function of material and laser parameters. The pulse duration dependence of the damage threshold has been extensively explored in fused silica for infrared laser pulses [12, 13, 16, 20–22]. Some groups have examined the effect of material band-gap [10] and laser wavelength [12], but a systematic study has not yet been conducted. More experiments are needed to quantitatively clarify the relative role of different ionization mechanisms for different laser and material parameters.

Most recent experiments in the femtosecond regime have measured the threshold for damage to the front surface of the sample. It has not been established that these surface thresholds are the same as bulk thresholds or whether they are lowered by contaminants or surface states that are more easily ionized than the bulk material. These easily ionized states could provide seed electrons for avalanche ionization, lowering the threshold. Von der Linde *et al* concluded that the surface thresholds they measured are most likely lowered by contamination or surface imperfections [23]. While the surface damage threshold is relevant for optimizing the damage threshold of first-surface optics and for surface micromachining, no theoretical work to date takes into account any surface effects, so establishing the importance of these effects through a systematic study of surface and bulk thresholds should be carried out.

In addition to establishing the correspondence between surface and bulk damage thresholds, one should establish the correspondence between the many different criteria that have been used to define the damage threshold. Du *et al* monitored the change in transmission of the laser pulse and the emission of light due to recombination of the plasma. Each spot in the sample was irradiated with only one laser pulse [20]. In contrast, Stuart *et al* optically inspected, under a Nomarski microscope, samples that had been irradiated by 600 successive pulses [12, 13]. Lenzner *et al* measured the volume of ablated material for 50 above-threshold pulses incident on each spot in the sample and extrapolated to zero ablated volume to obtain a threshold [10]. Varel *et al* used several *ex situ* techniques including Nomarski optical microscopy, atomic force microscopy and scanning electron microscopy to determine the threshold for single-shot ablation [21]. Tien *et al* used Nomarski microscopy of samples irradiated by single pulses [16], while Li *et al* measured the plasma emission from multiple shots on a single spot in the sample [24] to determine the threshold.

In addition to reconciling the different methods used to determine the damage threshold, the effect of multiple laser pulses hitting one spot in the sample must be addressed. Several groups have reported recently that, due to incubation effects, the threshold for multiple-shot experiments is lower than for single-shot experiments by a factor of two to four for femtosecond laser pulses [25, 26].

In this paper, we present measurements of the bulk damage threshold for femtosecond pulses in four different materials at two different laser wavelengths. We use a dark-field scattering technique, described in section 3.4, to determine the energy threshold for damage after irradiation with 3000 pulses. As described in section 2, by tightly focusing the pulses into the sample and making measurements of the damage threshold at multiple numerical apertures, we avoid the effects of self-focusing and optical aberrations, allowing the laser intensity at the focus to be accurately determined. For fused silica we find that the intensity threshold for bulk material damage for femtosecond pulses agrees very well with the thresholds for surface ablation found by other groups. The bulk threshold for CaF_2, however, is larger than the previously

measured surface threshold [21] by about a factor of two. The dependence of the intensity thresholds on laser wavelength and material band-gap suggests that avalanche ionization is responsible for producing most of the conduction band electrons for large band-gap materials, while photoionization is more important for low band-gap materials. Furthermore, we find that the photoionization by 400 nm pulses is best characterized as multiphoton ionization, while for 800 nm pulses the ionization is in the intermediate regime between multiphoton and tunnelling ionization.

2. Measuring bulk ionization thresholds

Early experiments on optical breakdown thresholds in the nanosecond and picosecond regime were done in bulk material [9, 15, 27–29]. The results of these experiments are, however, often complicated by the effects of self-focusing in the material [29]. More recently, the surface optical breakdown threshold for femtosecond pulses has been measured [10–13, 16, 20, 21, 23–26]. Researchers deliberately avoided bulk measurements because of the complications associated with self-focusing, dispersion and self-phase modulation. These effects modify the spatial and temporal profile of the laser pulse, making it difficult to determine the laser intensity to which the material is exposed. As mentioned above, however, it is not clear how well existing models, which do not take into account surface effects, describe the threshold for surface damage. In this section, we present a method for measuring the intensity threshold for bulk damage that avoids the complications due to self-focusing and focusing aberrations.

2.1. Complications with bulk threshold measurements: self-focusing

The primary difficulty with accurately determining the threshold for bulk optical breakdown and damage in transparent materials is to correctly determine the laser intensity at the observed threshold. The laser pulse energy, pulse duration and beam profile are measured outside the sample. If propagation through the sample did not affect any of these parameters, and if the focusing were aberration free, then the peak laser intensity would be simply related to the quantities that are measured. The high peak power of the laser pulses, however, induces nonlinear propagation effects that strongly distort the spatial and temporal profile of the laser pulse in a manner that is difficult to predict or model [31, 32]. For extremely short pulses, the dispersion in the material has to be taken into account to ensure the pulse is short at the focus inside the material.

Self-focusing is the most important nonlinear propagation effect that we must consider when determining bulk ionization thresholds because it strongly affects the laser intensity inside the material. Self-focusing results from the intensity dependence of the refractive index, given by [30]

$$n = n_0 + n_2 I \tag{3}$$

where n is the total refractive index, n_0 is the ordinary (low I) refractive index and n_2 is the nonlinear index. The spatial intensity profile in the laser pulse leads to a spatial refractive index profile: because n_2 is positive in most materials, the refractive index is higher at the centre of the beam compared to the wings. This variation in refractive index acts as a lens and focuses the beam.

Although the refractive index variation depends on the laser intensity, the strength of the self-focusing lens depends only on the peak power of the laser pulse [31]. This can be qualitatively understood as follows. Consider a collimated laser beam incident on a transparent material with sufficient power to self-focus inside the material. If the diameter of the incident laser beam is doubled, the laser intensity goes down by a factor of four resulting in a refractive index change that is smaller by a factor of four. The area of the self-focusing lens, however, is also increased by a factor of four. This increase in area compensates for the decrease in refractive index change, giving the same refractive power.

As the power in the laser pulse is increased, self-focusing becomes stronger until, at some critical power, it balances diffraction and a filament is formed. If the peak power of the laser pulse exceeds this critical power for self-focusing then catastrophic collapse of the laser beam to a singularity is predicted [31]. The critical power, P_{cr}, is given by

$$P_{cr} = \frac{3.77\lambda^2}{8\pi n_0 n_2} \tag{4}$$

where λ is the laser wavelength [31]. In reality, other mechanisms halt the collapse of the beam due to self-focusing. In particular, as the laser beam self-focuses, the intensity rises and eventually becomes sufficient to nonlinearly ionize electrons. The electron gas contributes a negative refractive index change that cancels the positive refractive index change produced by the intensity-dependent index and prevents further self-focusing [32].

Although much progress has been made in recent years, a comprehensive theory of nonlinear pulse propagation in transparent materials for pulses whose power exceeds the critical power is still lacking [32]. For laser powers that are less than about a quarter of the critical power for self-focusing, however, the change in spot size in the material due to self-focusing can be reliably calculated [29]. The laser intensity, I_{sf}, at the laser focus in the presence of weak self focusing increases with increasing peak power, P, according to [29]

$$I_{sf} = \frac{I}{1 - P/P_{cr}} \tag{5}$$

where I is the laser intensity in the material in the absence of self-focusing.

Because the change in laser intensity due to strong self-focusing cannot currently be calculated, strong self-focusing must be avoided when measuring bulk breakdown thresholds in order to reliably calculate the threshold intensity. To avoid strong self-focusing we make use of the fact that while the threshold for optical breakdown and damage depends on the laser intensity, the threshold for self-focusing depends on peak power. If the laser pulse is tightly focused into the material using an external lens, the intensity for optical breakdown can be reached with powers that are below the critical power for self-focusing [15, 33]. In transparent solids, the critical power is typically of the order of 1 MW [34, 35], and the intensity

threshold for bulk optical breakdown using a femtosecond laser pulse is about 10^{13} W cm^{-2} [5]. We can crudely estimate how tightly the laser beam must be focused to produce breakdown with power below the critical power by assuming the beam has a flat-top spatial profile. We then have

$$I = \frac{P}{\pi(d/2)^2} \tag{6}$$

where d is the diameter of the laser beam at the focus. Equation (6) shows that the laser must be focused to a spot size smaller than 3.6 μm to achieve breakdown below the critical power for self-focusing. With high numerical aperture (NA) microscope objectives, focal spots of well under 1 μm can be achieved, allowing the threshold for optical breakdown to be measured at laser powers that are more than an order of magnitude below the critical power for self-focusing. Under these circumstances, the correction due to self-focusing is small, and so the spot size of the laser at the focus follows from the numerical aperture of the objective and the wavelength of the laser. The intensity of the laser pulse at the focus can therefore be determined with confidence.

2.2. Complications with bulk threshold measurements: aberrations

While tight external focusing eliminates the difficulty in determining the peak laser intensity inside the material due to self-focusing, it brings other complications. With tight focusing it is difficult to directly measure the spot size of the laser beam inside the material. Instead, one must calculate the spot size based on the laser beam and focusing lens parameters. Focusing visible light to a spot size under 1 μm, however, requires focusing angles that go well beyond the paraxial approximation [36]. As a result, focusing aberrations can severely distort the focal spot. If we consider only beams that are incident at the centre of the focusing lens and that are parallel to the optic axis of the lens, the most important focusing aberration is spherical aberration, although chromatic aberration can also play an important role for wide-bandwidth pulses.

Microscope objectives are corrected to focus well through a 170 μm thick cover slip made of a glass with the appropriate refractive index ($n = 1.523$ at 589 nm) and Abbe number ($\nu = 56$)—one such glass is Corning 0211, a zinc-doped borosilicate glass. Because we are interested in investigating the breakdown threshold in materials with different band-gap, and therefore different refractive index, we must evaluate the effect of aberrations when focusing into materials with refractive indices different from that for which the objective is designed.

We modelled the effect of different refractive index materials by ray tracing. We reproduced the cone of converging rays produced by the microscope objective by assuming a perfect focus 170 μm beneath the surface of a cover slip and tracing rays back out of the cover slip. We then traced the cone back into a material with different refractive index, and varied the position of the material in and out of the cone to minimize the distortion of the focus. We find that for a 0.65 NA microscope objective one can find a focusing depth in a material with refractive index between 1.3 and 2.0 where the spread of the rays is less than 100 nm. Because this spread is significantly smaller than the diffraction-limited spot size, we take this small spread in the rays to indicate good focusing. The model predicts that the laser spot size increases dramatically when the laser is not focused to within 10 μm of the optimal depth in the material for the 0.65 NA objective. At lower NA, good focusing can be achieved over a greater range of focusing depths and refractive indices. For objectives with NA higher than 0.65 it becomes very difficult to avoid aberrations in any material other than a cover slip. Consequently we avoid using objectives with greater than 0.65 NA in all materials other than Corning 0211.

To ensure diffraction-limited focusing, we illuminate the back aperture of the microscope objective as uniformly as possible and completely fill it. The laser is focused into the sample at the best-focus depth determined from the model calculations. For microscope objectives with NA greater than about 0.5, we find that the threshold for optical damage increases dramatically when the laser is not focused at the optimal depth in the material, in agreement with the simulations. For the thresholds presented below, the laser is always focused at the depth where the lowest threshold for producing damage is achieved.

2.3. Measuring with multiple numerical apertures

To further ensure that we can accurately determine the laser intensity required to produce optical breakdown, we make measurements using multiple microscope objectives with different NA [5]. To first approximation, the energy, E_{th}, required to reach the intensity threshold for optical breakdown, I_{th}, scales linearly with the laser spot size (i.e. $E_{th} \propto I_{th}/\mathrm{NA}^2$). As discussed above, aberrations and self-focusing both cause a departure from this linear scaling. Aberrations play a role primarily at high numerical aperture (NA $\geqslant 0.4$), where the paraxial approximation breaks down [36]. Self-focusing, on the other hand, is more important at low numerical aperture (NA $\leqslant 0.65$) because the amount of self-focusing depends on the ratio of the peak power of the laser pulse to the critical power for self-focusing for the material, and because more energy is needed to reach the breakdown intensity at low NA, resulting in a higher peak power [31]. We try to minimize aberrations using the procedures described above, and make the small correction in equation (5) to the laser intensity to account for self-focusing. For diffraction-limited focusing in the presence of weak self-focusing, the energy required to reach the breakdown intensity is related to the NA of the objective by

$$E_{th} = \frac{I_{th}\tau\lambda^2}{\pi(NA)^2 + I_{th}\lambda^2/P_{cr}} \tag{7}$$

where τ is the laser pulse duration [5]. We measure the energy required to produce breakdown in the material for several objectives with NA between 0.25 and 1.4, and fit the observed energy thresholds to equation (7) with I_{th} as a free parameter.

Making measurements at multiple numerical apertures allows us to have very small corrections for self-focusing at high NA (where aberrations might be important), and to have low aberrations at low NA (where self-focusing becomes appreciable). If the energy threshold data over a range of

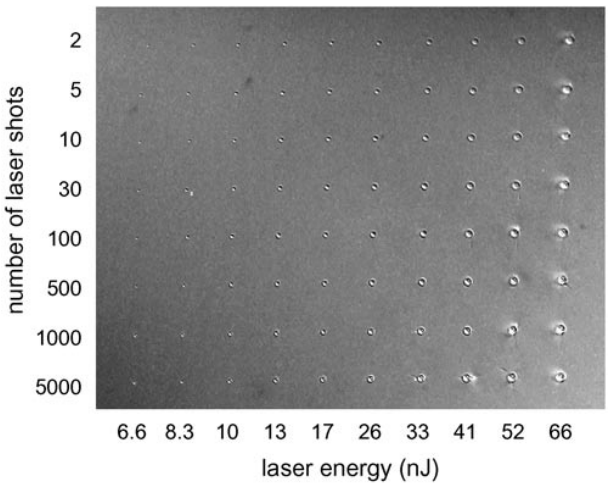

Figure 4. Differential interference contrast optical micrograph of structures produced with various energies and various numbers of 110 fs laser pulses focused by a 1.4 NA microscope objective in Corning 0211. The laser pulses are incident perpendicular to the plane of the image.

numerical apertures is well fitted by equation (7), which assumes no aberrations and weak self-focusing, then we can feel confident that we have accurately determined the intensity threshold.

3. Experimental techniques

We have used several different techniques to determine the energy threshold for producing permanent bulk damage in transparent materials. The band-gap and wavelength dependence data were aquired using a dark-field scattering technique that allows real-time assessment of the energy threshold for producing damage. Real-time assessment is critical for bulk measurements because the laser must be focused at the optimal depth in the material for the laser intensity to be reliably determined. We first briefly describe optical microscopy and transmission techniques for determining the threshold, then present a method for determining the critical power for self-focusing. Finally, we describe the dark-field scattering technique in detail. The three different techniques used to determine the threshold for damage yield results that agree within experimental error.

3.1. Damage threshold measurement: optical microscopy

One method for determining the threshold for optical damage is to produce arrays of structures made with varying laser energy and examine the array optically. Using differential interference contrast (DIC) microscopy with a 1.4 NA oil-immersion objective one can detect very small refractive index changes on a sub-micrometre scale. Figure 4 shows a DIC optical micrograph of an array of structures in Corning 0211 produced using 110 fs laser pulses from a 1 kHz laser focused into the bulk of the sample by a 1.4 NA oil-immersion objective. Each structure is made with a different combination of laser energy and number of laser shots.

No material change is observed for a laser pulse energy below 6 nJ, regardless of the number of shots incident on one spot in the sample. At 6.6 nJ we observe both single-shot and multiple-shot damage and so we conclude that the energy threshold for single-shot and multiple-shot damage in Corning 0211 at 1.4 NA is 6.6 nJ. When focusing with a 0.25 NA objective, however, we observe a decrease in the damage threshold for increasing number of incident laser pulses. Other researchers have observed a decrease in the surface ablation threshold of transparent materials with multiple-pulse irradiation [25, 26]. This lower threshold for multiple-shot damage indicates that incubation is important. During multiple pulse irradiation, small changes (e.g. colour centres) formed by the first few pulses may make it easier for later pulses to cause damage. More experiments on the effects of incubation are necessary to determine how important incubation effects are in bulk and surface damage and to determine whether our observed NA dependence applies to other materials.

3.2. Damage threshold measurement: transmission change

Alternatively, we can look for a drop in the transmission of the laser pulse due to absorption of laser energy by the material to determine the damage threshold. A similar technique has been used to determine the damage threshold at the surface [20]. Figure 5 shows the transmission of 110 fs laser pulses of different wavelength through fused silica as a function of incident laser energy. The laser pulses are focused into the sample by a 0.65 NA microscope objective. The energy at which the transmission begins to drop, corresponding to the energy threshold for optical breakdown and damage, is 25 nJ for 800 nm pulses. Using 400 nm pulses, we find an energy threshold of 20 nJ.

3.3. Self-focusing threshold

In order to make the correction in equation (5) to the laser intensity we must know the critical power for self-focusing. To determine this critical power, we measured the threshold for white-light continuum generation in various materials for a slow-focusing geometry (0.20 m focal length lens). Under such conditions, the threshold for critical self-focusing corresponds to the threshold for white-light continuum generation [34, 35]. Self-focusing does not depend on intensity, but only on the peak power [30]; thus the critical self-focusing threshold does not depend on the focusing geometry and is the same for fast and slow external focusing. The measured thresholds for critical self-focusing in fused silica (140 nJ at 400 nm and 580 nJ at 800 nm) are indicated in figure 5. The threshold energies for self-focusing are about an order of magnitude higher than the damage thresholds determined from the change in transmission, indicating that self-focusing does not play a dominant role in the damage formation.

For all measurements described in section 4, breakdown is achieved with a laser power that is below the critical power for self-focusing. In Corning 0211, for example, self-focusing is entirely negligible using numerical apertures of 1.0 and 1.4, while for 0.65, 0.45 and 0.25 NA self-focusing results in a 6, 10 and 20% decrease in spot size, respectively. In previous work, self-focusing played a more dominant role, complicating the determination of the threshold intensity for bulk optical breakdown [29].

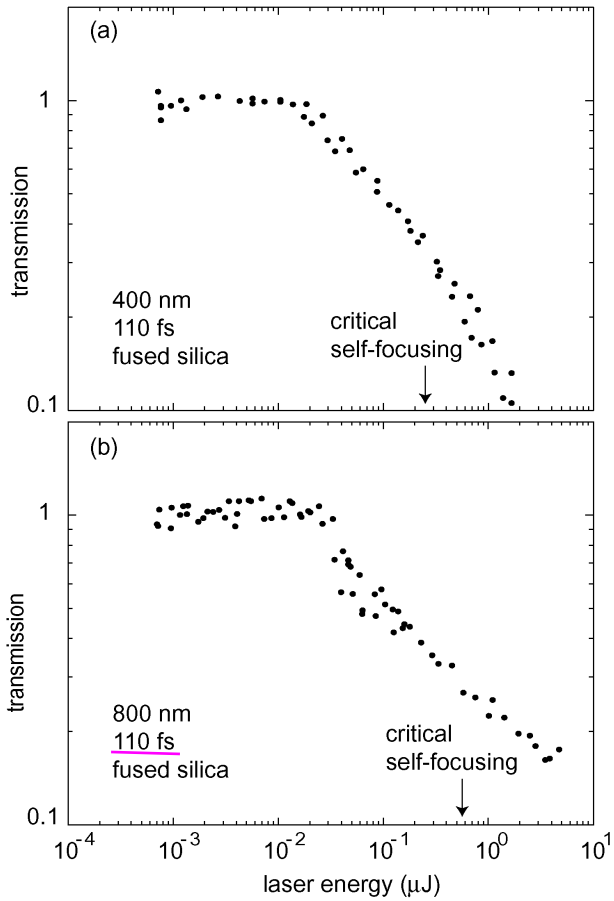

Figure 5. Transmission of (a) 400 nm and (b) 800 nm laser pulses of 110 fs duration focused by a 0.65 NA microscope objective into fused silica as a function of laser pulse energy. The arrows mark the energies corresponding to the critical power for self-focusing.

3.4. Damage threshold measurement: dark-field scattering

To study the material band-gap and laser-wavelength dependence of the damage threshold, we used the dark-field light scattering technique illustrated in figure 6. The primary advantage of this technique is that it is real time, allowing one to minimize the damage threshold by varying the focusing depth into the material, assuring that focusing aberrations are minimized. A 110 fs pump pulse is focused into the sample using a microscope objective with NA between 0.25 and 1.4. A He:Ne laser beam probes the pumped region of the sample. The He:Ne is focused into the sample at a lower NA than the femtosecond beam, so the beam waist at the focus is larger than that of the femtosecond beam. The directly transmitted He:Ne light is collected by a microscope objective and blocked with a circular beam block whose size is chosen so it just blocks the full He:Ne beam. When damage is produced in the sample by the femtosecond laser beam, some of the He:Ne light scatters into a larger cone angle than the directly transmitted light. The scattered light is collected by the microscope objective and focused around the beam block onto the detector.

It is critical that the objective used to collect the scattered He:Ne light have a higher acceptance angle (higher NA) than the cone angle of the unscattered He:Ne beam so that light scattered by the damage spot is collected and can be separated

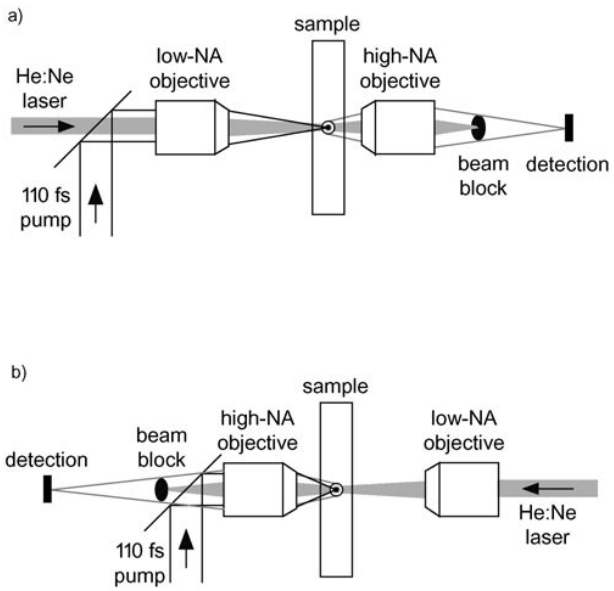

Figure 6. Dark-field scattering setup for determining the energy threshold for bulk damage using (a) low-NA and (b) high-NA objectives for focusing the femtosecond laser pulse.

from the directly transmitted He:Ne beam. Depending on the NA of the objective used to focus the femtosecond laser beam, we use one of two different setups. Figure 6(a) shows the setup used when the femtosecond beam is focused by an objective with NA lower than 0.45. The He:Ne beam co-propagates with the femtosecond laser and is focused into the material with the same objective. Because the He:Ne beam underfills the back aperture of the objective, it has a larger spot size in the material than the femtosecond beam. The scattered He:Ne light is collected by a 0.65 NA objective. Figure 6(b) shows the setup for focusing objectives with 0.45 NA or higher. The He:Ne probe propagates in the opposite direction to the femtosecond beam and is focused by a 0.25 NA objective into the sample. The He:Ne beam does not completely fill the back aperture of the objective. The scattered He:Ne light is collected by the objective which focuses the femtosecond beam. A dichroic mirror transmits the He:Ne light to the beam block and detector.

We determined the damage threshold by looking for an increase in the amount of He:Ne light reaching the detector after irradiation with 3000 femtosecond laser pulses on a single spot in the sample. The threshold was minimized by translating the sample in and out of the beam to find the best focus. After irradiation, the sample was translated laterally even if no damage was observed. Irradiating with multiple pulses as opposed to a single pulse forms a larger, more easily detected, damaged region. The sample is also perturbed mechanically by lightly tapping the sample mount during irradiation, producing an even larger volume of damaged material for above-threshold pulses, and further increasing the sensitivity of the technique. While incubation effects could lower the multiple-shot damage threshold compared to the single-shot damage threshold, as noted in section 3.1, we do not observe strong incubation effects in bulk damage thresholds with tight external focusing.

4. Ionization thresholds for femtosecond laser pulses

Using the dark-field scattering technique described in Section 3.4 we measured the energy required to produce damage in dielectric materials with different band-gap using 400 nm and 800 nm femtosecond pulses focused at various numerical apertures. Figures 7(a) and 7(b) show the dependence of the energy threshold for permanent damage for 400 nm and 800 nm pulses on numerical aperture. The lines represent fits to equation (7) using critical powers from the literature [34] or measured using the technique described in section 3.3. For Corning 0211, where no literature value is available and where direct measurement of the critical power is difficult because the available samples are very thin, the critical power at 800 nm was left as a free parameter. Our fits yield $P_{cr} = 1.5$ MW, in good agreement with the 1.6 MW value for BK7, a glass with composition and band-gap similar to Corning 0211. For Corning 0211, there are additional 800 nm energy thresholds at 1.0 NA (7.0 nJ) and 1.4 NA (5.0 nJ) that are not shown in figure 7, but were used in the fitting procedure. We used the known scaling of the critical power with laser wavelength (equation (4)) to obtain a value for Corning 0211 at 400 nm.

We do not observe damage in SF11 using 400 nm laser pulses with laser energy up to several times the threshold for other materials, even though we observe strong blue fluorescence from the pumped region of the sample. For 400 nm, absorption in SF11 requires only two photons and the two-photon absorption is efficient enough to cause significant absorption before the pulse reaches the laser focus. This absorption limits the peak laser intensity at the focus, preventing optical breakdown. Perhaps the electrons produced in front of the laser focus by two-photon absorption also act as a negative lens and defocus the laser pulse, further limiting the peak laser intensity.

From the fits to equation (7) we can determine the threshold intensity for optical breakdown and damage. Table 1 shows the critical powers for self-focusing and material band-gaps used in the fits and the threshold intensities resulting from the fitting. Note that while the threshold intensity for 400 nm pulses is lower than for that 800 nm pulses for Corning 0211 and fused silica, the reverse is observed for CaF_2.

The threshold for bulk damage in fused silica with 800 nm pulses is in good agreement with the literature values for surface damage using 110 fs laser pulses [10, 12]. Stuart *et al* observed a decrease of roughly a factor of two in the surface damage threshold in fused silica for 526 nm pulses compared to 1053 nm pulses for pulse durations of 300 fs and longer [12]. In contrast, we observe only a slight difference in the 400 nm and 800 nm bulk damage thresholds for fused silica. In CaF_2, the only other material for which literature values are available, we find that the threshold for bulk damage is higher than the literature value for the surface damage threshold [21].

5. Discussion

The pulse duration dependence of the threshold fluence required to produce material damage has been studied extensively [10, 12, 13, 20, 21]. Assuming that the electron density must reach the critical density to produce damage, this

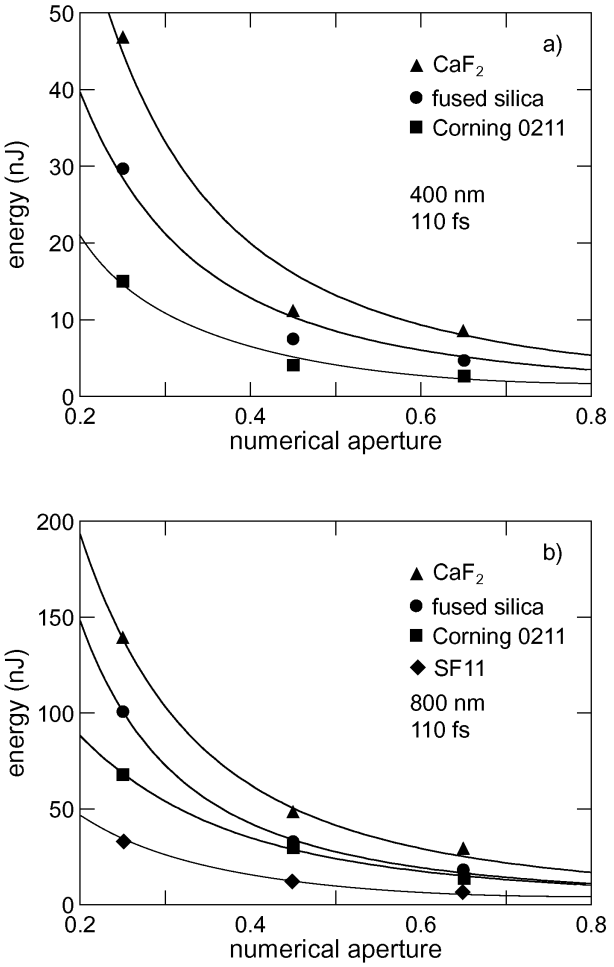

Figure 7. Energy threshold for permanent damage in SF11 (◆), Corning 0211 (■), fused silica (●) and CaF_2 (▲) as a function of NA for (a) 400 nm and (b) 800 nm, 110 fs laser pulses. Damage was not observed in SF11 using 400 nm light. Data points at 1.0 NA (7.0 nJ) and 1.4 NA (5.0 nJ) in Corning 0211 for 800 nm light are not shown. A fit to equation (7) is shown for each material.

dependence can be fitted to a rate equation for the electron density [10–13],

$$\frac{\mathrm{d}N}{\mathrm{d}t} = \alpha I N + P(I) \tag{8}$$

where N is the electron density, α is the avalanche ionization coefficient and $P(I)$ is the photoionization rate, typically taken to be $\sigma_k I^k$ [10, 12]. The multiphoton absorption coefficient, σ_k, and the avalanche ionization coefficient, α, are adjusted to fit to the data.

Because we have not determined the pulse duration dependence, we use Keldysh's theory for photoionization [8] to interpret the bulk damage thresholds listed in table 1. First, we calculate the Keldysh parameter (equation (1)), and determine whether the photoionization is best represented by a multiphoton or tunnelling ionization picture. Next, we calculate the electron density due to photonionization based on the rates predicted by Keldysh and compare this electron density to the critical density to determine the importance of avalanche ionization.

Table 1. Intensity threshold, I_{th}, for optical breakdown and damage in several transparent dielectrics for 400 nm and 800 nm, 110 fs laser pulses. The band-gap of the material and the critical powers, P_{cr}, used in the fit to equation (7) are also listed.

		400 nm		800 nm	
Material	Band gap (eV)	I_{th} (W cm^{-2})	P_{cr} (MW)	I_{th} (W cm^{-2})	P_{cr} (MW)
SF11	3.3	—	—	1.6×10^{13}	0.5
Corning 0211	4.4	1.5×10^{13}	0.4	2.8×10^{13}	1.5
Fused silica	7.5	2.9×10^{13}	1.1	3.2×10^{13}	4.3
CaF_2	10.2	4.8×10^{13}	1.9	4.3×10^{13}	7.4

Table 2. Keldysh parameter, γ, and electron density, N, due to multiphoton and tunnelling ionization calculated using the measured intensity thresholds for damage listed in table 1 and equation (37) in [30]. Avalanche ionization is not included in the calculation of the electron density. For comparison, the critical density is 6.9×10^{21} cm^{-3} (1.7×10^{21} cm^{-3}) for 400 nm (800 nm) light.

	400 nm		800 nm	
Material	γ	N (cm^{-3})	γ	N (cm^{-3})
SF11	—	—	1.2	3.0×10^{21}
Corning 0211	2.7	5.2×10^{21}	1.0	2.7×10^{21}
Fused silica	2.5	3.7×10^{20}	1.2	4.1×10^{19}
CaF_2	2.3	4.8×10^{19}	1.2	2.5×10^{18}

5.1. Multiphoton versus tunnelling ionization

Table 2 shows the Keldysh parameter and the electron density due to photoionization alone (i.e. avalanche ionization is not included) determined from the measured intensity thresholds for damage listed in table 1. We used the full Keldysh expression for $P(I)$, (equation (37) in [8]) to calculate the electron densities. At 400 nm, the Keldysh parameter for all materials is well within the multiphoton ionization regime. At 800 nm, however, the Keldysh parameter is in the intermediate region between multiphoton ionization and tunnelling ionization and so the approximation of the photonionization rate as $\sigma_k I^k$ in equation (8) is not well justified. In fact, from figure 2 we see that the multiphoton ionization rate is about an order of magnitude below the rate based on the full formula for 800 nm light in fused silica, and it may actually be better to characterize the photoionization at 800 nm as a tunnelling process. Lenzner *et al* also emphasized the importance of considering tunnelling ionization as an important ionization mechanism for short pulse durations [10].

5.2. Contribution of avalanche ionization

It is commonly assumed that a critical density plasma must be formed to produce material damage [10, 12, 20] because the plasma becomes strongly absorbing near the critical density, allowing a significant fraction of the laser pulse energy to be deposited into the material, leading to damage. We should therefore compare the electron densities listed in table 2 to the critical plasma density at the corresponding laser wavelengths. For a laser wavelength of 400 nm the critical density is 6.9×10^{21} cm^{-3}; at 800 nm it is 1.7×10^{21} cm^{-3}. For the low band-gap materials (SF11 and Corning 0211 at 800 nm and Corning 0211 at 400 nm) we see that photoionization alone is sufficient to produce a critical density plasma, suggesting that avalanche ionization plays a small role in the ionization process. This is in agreement with the results obtained by Lenzner *et al* for barium aluminium borosilicate glass which has a band-gap in the same range as SF11 and Corning 0211 [10]. For fused silica and CaF_2 the electron densities in table 2 fall well below the critical density at both 400 nm and 800 nm wavelength, indicating that avalanche ionization plays a more important role.

Equation (8) allows us to calculate the avalanche coefficients that are necessary to produce a critical density plasma in fused silica and CaF_2. To determine the photoionization rate, $P(I)$, we use the full Keldysh formula. This procedure yields the following values for the avalanche coefficients: 1.6 cm^2 J^{-1} (800 nm, fused silica), 2.0 cm^2 J^{-1} (800 nm, CaF_2), 1.3 cm^2 J^{-1} (400 nm, fused silica) and 1.4 cm^2 J^{-1} (400 nm, CaF_2). The weak wavelength dependence of the avalanche ionization coefficient is in agreement with the results of Stuart *et al* [12]. The avalanche coefficient for fused silica at 800 nm, however, is smaller than that found by other researchers (values range from 4.0 cm^2 J^{-1} to 10 cm^2 J^{-1}), perhaps indicating that the electron densities calculated using the Keldysh rates are too high, as suggested by Lenzner *et al* [10]. Using the multiphoton ionization rate suggested by Lenzner, $\sigma_6 = 6.0 \times 10^8$ cm^{-3} ps^{-1} (cm^2 TW^{-1})^6, we find from our measured threshold intensity an avalanche ionization coefficient of 4.5 cm^2 J^{-1}, in good agreement with literature values.

6. Conclusions

In this paper, we present a method for accurately determining the intensity threshold for producing damage in bulk transparent materials by laser irradiation. The laser pulse is tightly focused into the material so that the threshold intensity is reached at low peak power, minimizing the self-focusing. Using this technique, we determined, for 110 fs laser pulses, the laser-wavelength and material band-gap dependence of the threshold intensity for bulk damage. Our results indicate that avalanche ionization produces most of the free electrons for large band-gap materials, while photoionization produces a significant fraction of the electron density for small band-gap materials. At 400 nm, photoionization is a multiphoton absorption process, while at 800 nm photoinoization is caused by tunnelling. More experimental and theoretical work is necessary to determine the photoionization rates and the scaling of the avalanche ionization rate with laser intensity as well as establish the validity of Keldysh's theory.

As figure 7 shows, the energy thresholds for 0.65 NA focusing are under 50 nJ for all materials studied in this paper. This energy is achievable with cavity-dumped and

long-cavity femtosecond laser oscillators, opening the door to unamplified micromachining [5, 37, 38]. The threshold in Corning 0211, at 5 nJ for 1.4 NA focusing, is within the range of commercially available laser systems. Using unamplified lasers for micromachining greatly reduces the cost and complexity of the laser system, and the high repetition rate of these lasers allows one to achieve higher machining speeds than are possible with amplified systems.

Acknowledgments

We thank Professors N Bloembergen and H Ehrenreich, and J B Ashcom for useful discussions. This work was funded by the National Science Foundation.

References

[1] Bloembergen N 1997 *J. Nonlin. Opt. Phys. Mater.* **6** 377
[2] Perry M D and Mourou G 1994 *Science* **264** 917
[3] Liu X, Du D and Mourou G 1997 *IEEE J. Quantum Electron.* **33** 1706
[4] Glezer E N, Milosavljevic M, Huang L, Finlay R J, Her T-H, Callan J P and Mazur E 1996 *Opt. Lett.* **21** 2023
[5] Schaffer C B, Brodeur A, Garcia J F and Mazur E 2001 *Opt. Lett.* **26** 93
[6] Davis K M, Miura K, Sugimoto N and Hirao K 1996 *Opt. Lett.* **21** 1729
[7] Homoelle D, Wielandy S, Gaeta A L, Borrelli N F and Smith C 1999 *Opt. Lett.* **24** 1311
[8] Keldysh L V 1964 *Zh. Eksp. Teor. Fiz.* **47** 1945 (Engl. transl. *Sov. Phys.–JETP* **20** 1307 (1965))
[9] Jones S C, Braunlich P, Casper R T, Shen X-A and Kelley P 1989 *Opt. Eng.* **28** 1039
[10] Lenzner M, Krüger J, Sartania S, Cheng Z, Spielmann Ch, Mourou G, Kautek W and Krausz F 1998 *Phys. Rev. Lett.* **80** 4076
[11] Du D, Liu X and Mourou G 1996 *Appl. Phys.* B **63** 617
[12] Stuart B C, Feit M D, Herman S, Rubenchik A M, Shore B W and Perry M D 1996 *Phys. Rev.* B **53** 1749
[13] Stuart B C, Feit M D, Herman S, Rubenchik A M, Shore B W and Perry M D 1996 *J. Opt. Soc. Am.* B **13** 459
[14] Yu P Y and Cardona M 1996 *Fundamentals of Semiconductors* (Heidelberg: Springer) p 296
[15] Bloembergen N 1974 *IEEE J. Quantum Electron.* **10** 375
[16] Tien A-C, Backus S, Kapteyn H, Murnane M and Mourou G 1999 *Phys. Rev. Lett.* **82** 3883
[17] Thornber K K 1981 *J. Appl. Phys.* **52** 279
[18] Wood R M 1986 *Laser Damage in Optical Materials* (Boston: Hilger)
[19] Soileau M J, Williams W E, Van Stryland E W, Boggess T F and Smirl A L 1984 *Natl Bur. Stand. (US) Spec. Publ.* **669** 387
[20] Du D, Liu X, Korn G, Squier J and Mourou G 1994 *Appl. Phys. Lett.* **64** 3071
[21] Varel H, Ashkenasi D, Rosenfeld A, Herrmann R, Noack F and Campbell E E B 1996 *Appl. Phys.* A **62** 293
[22] Kautek W, Krüger J, Lenzner M, Sartania S, Spielmann Ch and Krausz F 1996 *Appl. Phys. Lett.* **69** 3146
[23] von der Linde D and Schüler H 1996 *J. Opt. Soc. Am.* B **13** 216
[24] Li M, Menon S, Nibarger J P and Gibson G N 1999 *Phys. Rev. Lett.* **82** 2394
[25] Rosenfeld A, Lorenz M, Stoian R and Ashkenasi D 1999 *Appl. Phys.* A **69** (Suppl) S373
[26] Lenzner M, Krüger J, Kautek W and Krausz F 1999 *Appl. Phys.* A **69** 465
[27] Smith W L, Bechtel J H and Bloembergen N 1977 *Phys. Rev.* B **15** 4039
[28] Sparks M, Mills D L, Warren R, Holstein T, Maradudin A A, Sham L J, Loh E Jr and King D F 1981 *Phys. Rev.* B **24** 3519
[29] Soileau M J, Williams W E, Mansour N and van Stryland E W 1989 *Opt. Eng.* **28** 1133
[30] Boyd R W 1992 *Nonlinear Optics* (Boston: Academic)
[31] Marburger J H 1975 *Prog. Quantum Electron.* **4** 35
[32] Gaeta A L 2000 *Phys. Rev. Lett.* **84** 3582, and references therein
[33] Yablonovitch E 1971 *Appl. Phys. Lett.* **19** 495
[34] Brodeur A and Chin S L 1998 *Phys. Rev. Lett.* **80** 4406
[35] Brodeur A and Chin S L 1999 *J. Opt. Soc. Am.* B **16** 637
[36] Siegman A E 1986 *Lasers* (Sausalito, CA: University Science Books) p 630
[37] Cho S H, Morgner U, Kartner F X, Ippen E P, Fujimoto J G, Cunningham J E and Knox W H 1999 *OSA Tech. Digest: Conf. on Lasers and Electro Optics* vol 99, p 470
[38] Libertun A R, Shelton R, Kapteyn H C and Murnane M M 1999 *OSA Tech. Digest: Conf. on Lasers and Electro Optics* vol 99, p 469